INTERNATIONAL JOURNAL FOR NUMERICAL AND ANALYTICAL METHODS IN GEOMECHANICS
Int. J. Numer. Anal. Meth. Geomech., 2003; **27**:859–877 (DOI: 10.1002/nag.304)

A new approach for calculating strain for particulate media

Catherine O'Sullivan[1,*,†,‡], Jonathan D. Bray[2,§] and Shaofan Li[2,¶]

[1] *Department of Civil Engineering, University College Dublin, Earlsfort Terrace, Dublin 2, Ireland*
[2] *Department of Civil and Environmental Engineering, University of California, Berkeley, 440 Davis Hall, Berkeley, CA 94720-1710, U.S.A.*

SUMMARY

Discrete element modelling is a viable alternative to conventional continuum-based analysis for analysing problems involving localized deformations of particulate media. However, to aid in the interpretation of the results, it is useful to express the results of discrete element analyses in terms of the continuum parameters of stress and strain. A number of homogenization methods have been proposed to calculate strain in discrete systems; however, two significant limitations of these methods remain. First, none of these methods incorporate particle rotation effects satisfactorily, although significant particle rotation occurs in shear bands in both physical tests and numerical simulations of granular materials. Additionally, observations of the particle displacement fields in shear bands in granular materials indicate that the displacements within the localizations are erratic. Consequently, existing linear, local interpolation approaches produce substantial variations in the strain values calculated in adjacent elements in the region of localization, hindering clear visualization of the strain localization as it evolves. A new method of domain discretization for calculating strain is proposed. This method is capable of capturing particle rotation and employs a non-local meshfree interpolation procedure capable of smoothing the erratic displacements in strain localizations, which better defines their evolution. The proposed method is validated for problems involving both two and three dimensions. A number of methods are compared with the proposed method and pertinent insights are made. Copyright © 2003 John Wiley & Sons, Ltd.

KEY WORDS: granular materials; discrete element methods; strain; kinematic homogenization; numerical simulations

INTRODUCTION

Discrete element methods are promising numerical tools for analysing a variety of problems involving particulate media. However, continuum methods continue to be the prevailing numerical approach in research and practice. A discrete element simulation calculates inter-particle contact forces and particle displacements, while continuum analyses typically provide results in terms of stress and strain. Various homogenization methods have been developed to

*Correspondence to: C. O'Sullivan, Department of Civil Engineering, University College Dublin, Earlsfort Terrace, Dublin 2, Ireland.
† E-mail: catherine.osullivan@ucd.ie
‡ Lecturer
§ Professor
¶ Assistant Professor

Received 27 December 2002
Revised

'link' the two approaches, and allow the results of discrete element simulations to be compared with those from the more familiar continuum-based analyses. Static averaging operators can be used to calculate stress values from the contact forces in discrete element analyses, and kinematic averaging operators are used to calculate strain. While the calculation of stress for a discrete system is well defined (e.g., Reference [1]), there is no single definitive approach for kinematic averaging to calculate strain across particulate media. In this paper, some new approaches for calculating strain, specifically considering problems involving strain localization or shear bands, are proposed.

As an introduction to the kinematic homogenization methods proposed in this paper, a brief overview of recent research into the development of kinematic homogenization methods is presented. A new discretization approach for kinematic homogenization, capable of capturing particle rotations, is then proposed. The two-dimensional linear triangulation 'finite element' interpolation approach for kinematic homogenization is extended to three dimensions. An alternative, higher-order, non-local 'meshfree' approach is implemented and validated for both two- and three-dimensional homogenization. Finally, the proposed methods are used to analyse the results of a discrete element simulation of a biaxial compression test on a dense, two-dimensional specimen of disks, where a shear band develops after its peak strength is mobilized.

BACKGROUND AND MOTIVATION

Recent publications that offer detailed critical examinations of the available methods for kinematic homogenization include References [2–4]. For all these approaches, the particle displacements and rotations are calculated using a discrete element method. The homogenization methods are applied as a post-processor to the discrete element analysis to obtain an average displacement gradient value for a collection of particles. The strain values are then calculated from the homogenized displacement gradients. For many engineering applications, an infinitesimal strain field is adequate to describe the deformation state. However, for finite deformation problems in general, and for problems with large localized deformations in particular, an infinitesimal strain field is no longer an appropriate measure for deformation. The definition of the finite strain tensor depends on whether the deformation measure is related to the reference (original) configuration or the current configuration [5]. When the deformation measure is related to the reference configuration, the Green strain tensor, E_{ij}, is often used, which can be expressed as

$$E_{ij} = \frac{1}{2}(u_{j,i} + u_{i,j} + u_{k,i}u_{k,j}) \tag{1}$$

where $u_{i,j}$ is the displacement gradient tensor. Refer to Zienkiewicz and Taylor [5] for a more detailed explanation. The undeformed particle coordinates are selected as the reference configuration for all of the simulations presented here. In addition, the strain contours are plotted on the reference configuration in all cases.

Several kinematic homogenization methods have been proposed in recent years. For problems involving strain localizations, it appears that the spatial discretization type approaches are the most appropriate of the methods currently used for calculating strain in a discrete system. In the spatial discretization type approaches, a graph, or nodal network, connecting the particles is created; typically this graph is constructed by considering the particle centroidal

coordinates. The incremental displacement gradient is calculated by considering the relative incremental displacement along each edge of the graph, and assuming a linear variation in the displacement values between adjacent nodes. The spatial discretization methods can be decomposed into two steps: (1) discretize the domain to construct the graph, and (2) interpolate between adjacent nodes to calculate the displacement gradient. While earlier approaches differ in the way in which the graph system is set-up, they all use linear interpolation to calculate the displacement gradients. Recent evaluations of various kinematic averaging operators (e.g. References [2–4]) indicate that the strain calculated using the spatial discretization approaches generally gives a good match to globally applied strain values.

Both Thomas [6] and Dedecker *et al*. [3] used approaches based on triangulation of the granular medium and displacement of the particle centroids. Then, in each triangular element, a linear variation in displacement is assumed. Recognizing the similarity with the finite element constant strain triangle, the displacement gradient can be easily calculated. As demonstrated by Thomas [6], the evolution of strain localizations within the granular material can be monitored using homogenized strain values based on this triangular finite element-type interpolation. While all of the methods discussed here have been shown to be theoretically applicable in three dimensions, there have been few, if any, publications considering three-dimensional implementations.

Other kinematic homogenization methods that have been proposed include an energy-based method [7] and best fit-type approaches (e.g. Reference [8]). Cambou *et al*. [4] and Dedecker *et al*. [3] clearly demonstrate that Calvetti's energy method, which equates the strain energy in an equivalent continuum to the energy stored in the contacts of a discrete system, yields inaccurate estimates of strain. The best fit-type approach proposed by Liao *et al*. [8] seeks a translation field that is close to the calculated displacements of the discrete system. A functional form for the translation field is assumed, and the method of least squares is then used to determine the coefficients for the equation. This approach is not well suited to problems involving localizations, because a highly complex functional form would be required to capture the displacement field.

All of the existing 'equivalent continuum' approaches discretize the domain by considering only the particle centroids and neglect particle rotations. The experimental studies of Oda and Kazama [9], amongst others, have indicated that a high gradient of particle rotation appears at the boundaries of shear bands. Based on the results of experiments on 2-D rod assemblies, Dedecker *et al*. [3] concluded that a prevailing phenomenon to explain irrecoverable global strain is rolling of the particles around each other. The work of Oda and Kazama [9] and Iwashita and Oda [10] further explored the significance of particle rotation effects on the response of granular materials in two dimensions. A key finding of these studies is that particles within the shear band experience significant rotation. Thomas [6] also outlined the necessity to include particle rotations in the kinematic averaging operator. Dedecker *et al*. [3] proposed a homogenization method based on the contact displacements that incorporate rotation. This approach is limited, as rotational effects can only be included along branches of the graph connecting the particle centroids where the particles are in contact. Furthermore, extrapolation of this approach to three dimensions is non-trivial.

One limitation associated with the linear interpolation employed in the spatial discretization approaches is that the associated interpolation error is $\boldsymbol{O}(\boldsymbol{h})$, where $\boldsymbol{h}$ is the size of the discretization. Additionally, the strain values at a given point are calculated only based on the displacements of immediately adjacent particles. Numerical simulations (e.g. Reference [11])

have shown that the particle displacements within the shear zone are erratic. The linear interpolation approaches will therefore give strain values with substantial inter-element variation, making quantification of strain within the localization tenuous. While recognizing that such disorder is a feature of the localization, it may be desirable to average or smooth the displacement gradient, so that one may be able to estimate the overall strain at the region with a strong or weak discontinuity. In this way the evolution of the strain in the localization zone can be more easily examined. Thomas [6] discussed the difficulties associated with defining the location of the discontinuity, e.g. plotting the strain contours is complicated by the inter-element variation in strain values. A higher-order interpolation approach would reduce the interpolation error and smooth any discontinuous fields (associated with erratic particle movements) enabling them to become regular concentration fields.

FORMULATION OF PROPOSED STRAIN CALCULATION METHODS

New discretization approach to capture the effects of particle rotation

As discussed previously, the equivalent continuum approaches that discretize the domain by considering the particle centroidal coordinates are a validated method for kinematic homogenization. However, particle rotations cannot be accounted for using these approaches. A schematic diagram illustrating the effects of particle rotation on the calculated strain values is illustrated in Figure 1(a). When a particle experiences a finite amount of rotation, the displacements of points on the edge of the particle may differ substantially from the centroidal

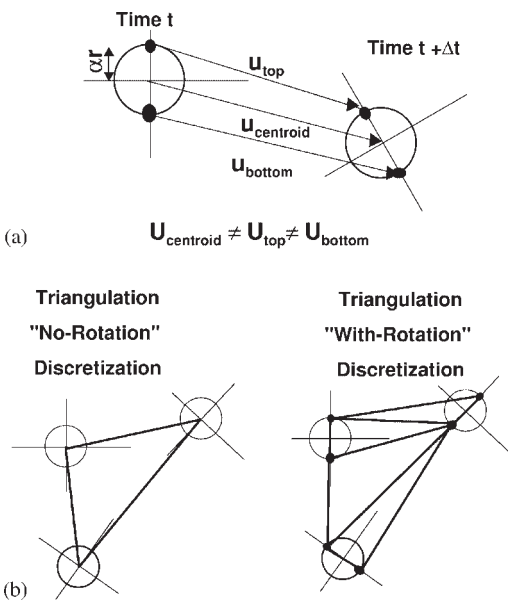

Figure 1. Schematic diagram of proposed discretization approach to capture the effects of particle rotation on local strain values.

displacements, consequently, the displacement gradient values calculated considering the centroidal coordinates alone do not capture the actual strains that the assembly of particles is experiencing.

The 'no rotation' discretization approach that has been used in previous linear interpolation methods is compared schematically with the proposed 'rotational' discretization approach in Figure 1(b). The original 'no rotation' discretization approach considers only the centroidal displacements. In the proposed 'rotational' discretization method, the displacements of two points located at a distance from the particle centroid are tracked. A similar idea was used by Bardet [1] in the boundary displacement method. The displacement of these points is a function of both the centroidal displacements, as well as the particle rotations. The details of the approach will differ slightly depending on whether the analysis is two-dimensional or three-dimensional.

Considering the two-dimensional case, the coordinates of the two 'tracked' points ($j = 1, 2$) for each particle are as follows:

$$\begin{bmatrix} u(j) \\ v(j) \end{bmatrix} = \begin{bmatrix} u(0) \\ v(0) \end{bmatrix} + \alpha(-1)^j r \begin{bmatrix} \sin\omega \\ \cos\omega \end{bmatrix} \tag{2}$$

where $u(j)$ and $v(j)$ are the co-ordinates of the tracked points, $u(0)$ and $v(0)$ are the co-ordinates of the particle centroid, ω is the accumulated particle rotation, r is the particle size (radius for circular particles), and α is a constant of proportionality to relate the position of the monitoring point to the particle size (typically, set to 0.9). All of these variables are easy to monitor in a two-dimensional discrete element analysis.

For the three-dimensional case, the coordinates of the two 'tracked' points ($j = 1, 2$) are given by the intersection of the principle axis of inertia of the particle with the particle boundary. The time integration approaches for three-dimensional analysis generally keep track of the orientation of the principal axes of inertia (e.g. Reference [12]). Therefore, as with the two-dimensional case, no additional calculations are required within the body of the discrete element code.

Implementation of existing two-dimensional linear approach in three dimensions

Previous discussions of linear interpolation approaches (e.g. References [4,6]) have considered two-dimensional implementations only. The method proposed by Thomas can be extended to three dimensions using constant strain tetrahedra in lieu of the constant strain triangles. The basic principles of the approach are outlined here. The use of tetrahedral elements in three-dimensional finite element analysis is described by Zienkiewicz and Taylor [13]. The four nodes of a tetrahedron are the particle centroids, or when rotations are considered, the measured points. Using linear interpolation, the displacement at any point (with co-ordinates (x, y, z)) in the tetrahedron can be expressed as

$$\begin{aligned} u(x, y, z) &= \beta_1 + \bar{a}_{11}x + \bar{a}_{12}y + \bar{a}_{13}z \\ v(x, y, z) &= \beta_2 + \bar{a}_{21}x + \bar{a}_{22}y + \bar{a}_{23}z \\ w(x, y, z) &= \beta_3 + \bar{a}_{31}x + \bar{a}_{32}y + \bar{a}_{33}z \end{aligned} \tag{3}$$

where u, v and w represent the incremental displacements in the x, y and z directions, respectively, the $\bar{a}_{ij}$ values are the averaged displacement gradients for the tetrahedron, and the

β values are arbitrary constants. The $\bar{a}_{ij}$ values are constant across each tetrahedron. The strain values are then calculated using Equation (1).

Implementation of meshfree interpolation approach in two and three dimensions

For a better interpretation of discrete element modelling results, an ideal homogenization procedure would use a higher order interpolation field ($C^n(\Omega)$, $n >= 1$, where $C^n(\Omega)$ represents a function space, in which functions have continuous n-th order derivatives) with non-local character. Such an approach would provide a smooth interpolation basis capable of capturing the high deformation gradient field inside the shear band (and hence the strain field), while also eliminating the high inter-element variation in strain values associated with local (linear) interpolation based homogenization (as documented by Thomas [6]). A suitable technique was found in the literature relating to the 'meshfree' methods [14,15]. Meshfree methods have been used by researchers to simulate strain localization problems (e.g. Reference [16]). In fact, it has been found that the meshfree interpolants are particularly effective in simulating strain localization under large deformation.

In contrast to the finite element interpolation, meshfree interpolation is a non-local data fitting algorithm that is entirely based on nodes, or particles, it does not require either elements or a mesh. The commonly used meshfree shape functions can interpolate over a set of randomly distributed particles in space with optimal accuracy. A shortcoming of the spatial discretization, graph-based approaches is that they impose a mesh constraint on the discrete system while interpreting the DEM data. The advantage of using meshfree interpolants to homogenize DEM data is that one can interpret DEM data without imposing an additional topological constraint to the system.

In the current study, we are only utilizing meshfree shape functions to homogenize or to smooth the discrete data set obtained from DEM analyses. Other aspects of the meshfree methods are not considered here. For a more detailed description of the meshfree methods readers may consult References [14,15]. The application of meshfree methods to geotechnical applications was explored by Murakami *et al*. [17], who used EFGM (element-free Galerkin method) analysis to analyze consolidation. A previous, but limited, investigation of the application of meshfree shape functions to strain calculation in discrete element simulations is described by Horner [18]. Horner's study was largely limited to a linear shape function, and the strain values were calculated by first calculating the spatial velocity gradient.

A schematic diagram of the approach used in the non-linear interpolation is illustrated in Figure 2. The displacement values are known from the DEM simulation. A rectangular grid is generated to serve as a referential continuum discretization over the volume of particles under consideration. The interpolated displacements and displacement gradients are then calculated at these grid points using the meshfree interpolants. A compact support is associated with each particle that defines its zone of influence, i.e. the area over which the particle contributes to the interpolated displacement field, and hence the average strain field. For the analyses discussed here the compact support associated with each particle is a multiple of the particle radius. The particular meshfree interpolant adopted is the meshfree interpolant used in the so-called reproducing kernel particle method (RKPM) [19].

At an arbitrary position inside a particulate aggregate, the displacement field can be expressed in terms of the nodal displacements at the tracked points. That is the interpolation is sampled at

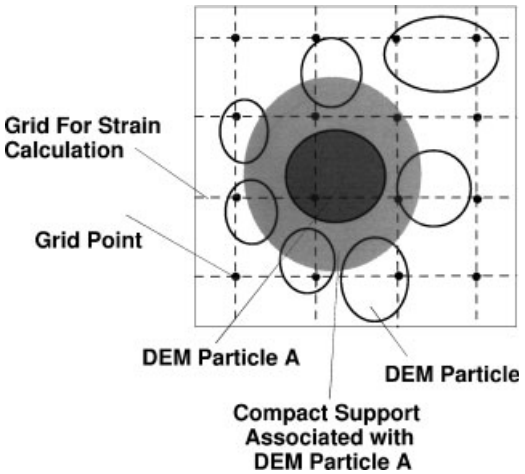

Figure 2. Schematic diagram of meshfree interpolation approach.

the tracked points,

$$u(x) \cong \sum_{i=1}^{N_p} K_\rho(x - x_i, x) u(x_i) \Delta V_i \tag{4}$$

where N_p is the number of tracked points, ΔV_i is the nodal weight, and the term $K_\rho(x - x_i, x)$ is given by

$$K_\rho(x - x_i, x) = C_\rho(x - x_i, x) \Phi_\rho(x - x_i, x) \tag{5}$$

where $C_\rho(x - x_i, x)$ is a correction function to reduce the interpolation error, and

$$\Phi_\rho(x) = \frac{1}{\rho^d} \phi\left(\frac{x}{\rho}\right) \quad d = 2, \text{ for 2D and } d = 3, \text{ for 3D} \tag{6}$$

is a compact supported window function, where ρ is the dilation parameter that defines the size of the window function. In this paper, the cubic spline function is chosen as the compact supported window function,

$$\phi(x) = \frac{1}{6}(x + 2)^3 \quad -2 \leqslant x \leqslant -1 \tag{7a}$$

$$\phi(x) = \frac{2}{3} - x^2(1 + x/2) \quad -1 \leqslant x \leqslant 0 \tag{7b}$$

$$\phi(x) = \frac{2}{3} - x^2(1 - x/2) \quad 0 \leqslant x \leqslant 1 \tag{7c}$$

$$\phi(x) = \frac{1}{6}(x - 2)^3 \quad 1 \leqslant x \leqslant 2 \tag{7d}$$

$$\phi(x) = 0 \quad \text{otherwise} \tag{7e}$$

In higher dimensions, the window function is formed as a Cartesian product, i.e.:

$$\phi(x, y) = \phi(x)\phi(y)$$
$$\phi(x, y, z) = \phi(x)\phi(y)\phi(z) \tag{8}$$

To calculate the meshfree shape function, $K_\rho(x - x_i, x)$, at each sample point i (tracked point) the size of the compact support must be known. In two dimensions, the compact support is a circle centered at the tracked point with a typical radius $w = 2r$, where r is the radius of the circular particle associated with the tracked node. While in three dimensions, the compact support is a sphere of radius with a typical radius $w = 2r$, where r is the radius of the spherical particle associated with the tracked node.

There are several ways to calculate the correction function. The simplest way is to use the condition of partition of unity,

$$\sum_{i=1}^{N_p} C_\rho(x - x_i, x)\phi_\rho(x)\Delta V_i = 1 \tag{9}$$

to determine $C_\rho(x - x_i, x)$ at an arbitrary point x. To obtain higher order interpolation accuracy, one may enforce certain 'reproducing conditions' and find the correction function by solving a moment equation. For details, readers may consult Liu *et al*. [20].

Each tracked point is also associated with a weight, ΔV_i, which may be calculated by first triangulating the system in terms of all the tracked points. Then each tracked point is a vertex of a number of triangles. The weight, ΔV_i, can then be determined as

$$\Delta V_i = \frac{1}{N_v} \sum_{k=1}^{N_T} \Delta\Omega_k \tag{10}$$

where $\Delta\Omega_k$ represents the area of a triangle with a vertex at the tracked point i, N_T is the total number of triangles with vertices at point i, and N_v is the number of vertices per triangle (N_v is 3 in two dimensions). Similarly, in three dimensions, the system was divided into tetrahedra, and the incremental volume associated with particle i, was calculated by considering the tetrahedra with vertices at point i (N_v is 4 in three dimensions).

The two-dimensional shape function described above is plotted in Figure 3(a). Visualization of the 3-D shape function is non-trivial. In Figure 3(b), the variation in magnitude of the shape function is illustrated with shading. The region with darker color indicates where the shape function value approaches zero, while white or bright color indicates the region where the shape function is a maximum.

VALIDATION OF PROPOSED METHODS

Two-dimensional case

The approach proposed by Dedecker *et al*. [3] and Bagi and Bojtar [2] is used here to validate the proposed kinematic averaging methods. A biaxial compression test on a disk specimen was simulated using the two-dimensional DEM code, PFC-2D [21]. The test specimen is illustrated in Figure 4(a). The specimen contained 1052 circular disk particles, with a mean particle radius of 0.174 m and a standard deviation of 0.014 m. The particle density was 2.6×10^4 kg/m^3.

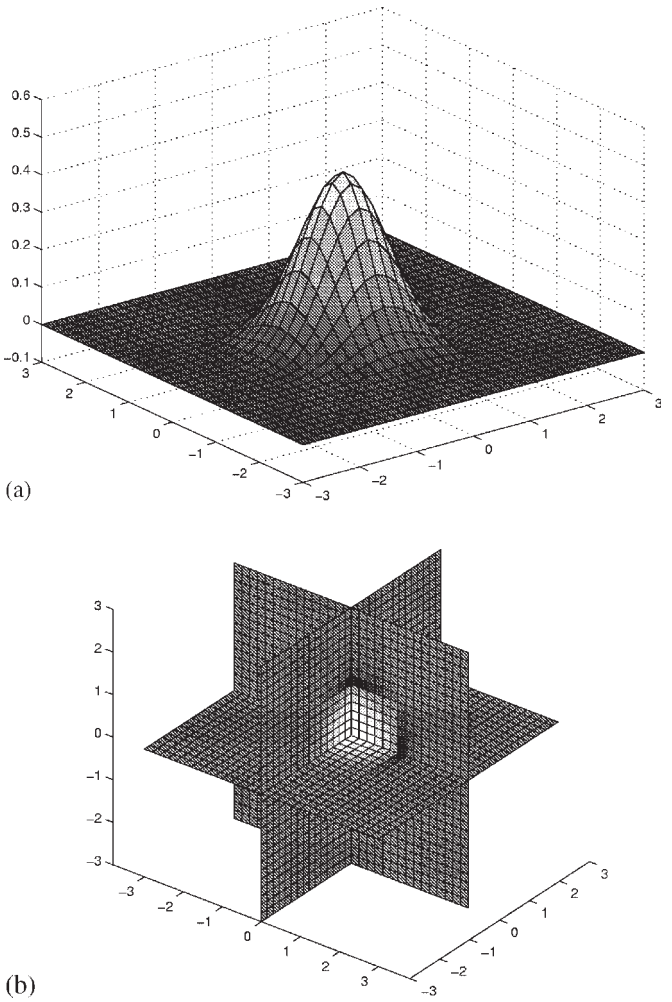

Figure 3. Shape functions for meshfree interpolation: (a) two dimensions and (b) three dimensions.

Contact was modelled using linear normal and shear springs with a stiffness of 5×10^7 N/m. A PFC damping coefficient of 0.2 was used, and the interparticle coefficient of friction was 0.324. The specimen was enclosed by four rigid walls. Using a servo-controlled system, the wall velocities were initially adjusted to attain an isotropic stress condition with $\sigma_{xx} = \sigma_{zz} = 50.7$ kPa. Once the specified isotropic stresses were achieved, the top rigid boundary was moved downwards with a constant velocity, while adjusting the velocity of the lateral boundaries to maintain the specified σ_{xx} values. The resulting specimen response is illustrated in Figure 4(b). The points at which the strain calculation methods were applied for the validation study are identified in Figure 4(b). The global axial and lateral displacement gradients were calculated from the boundary displacements. While the rigid, lateral boundaries inhibit the development of free localizations in the specimen, this validation approach is an effective way to demonstrate the accuracy of the kinematic averaging operators in both directions.

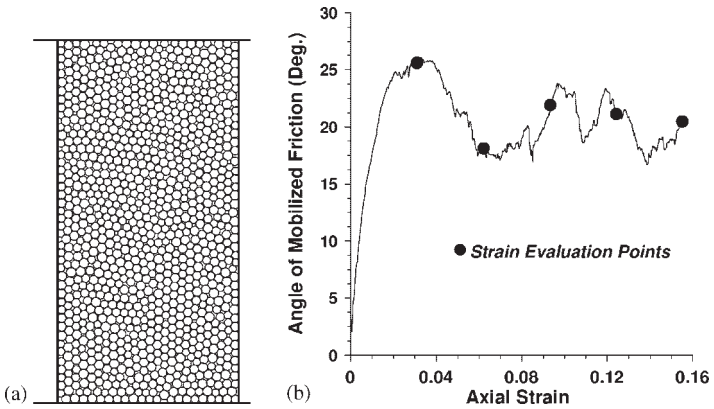

Figure 4. Validation of 2-D kinematic averaging approaches: (a) test specimen configuration and (b) specimen response.

Four kinematic homogenization approaches were considered; linear interpolation using both the 'no-rotation' and 'rotational' discretizations, and non-linear meshfree interpolation using both discretization approaches. For the 'rotational' discretization, the measured points were located at 0.9 times the disk radius from the disk centroid. The grid used in the non-linear interpolation had 40 points in the x-direction and 80 points in the y-direction. The radius of the window support for each disk is twice the disk radius. The average global displacement gradients, a_{xx}^{global} and a_{zz}^{global}, as calculated from the boundary conditions, are compared with the mean displacement gradients, $\bar{a}_{xx}$ and $\bar{a}_{zz}$, in Figure 5. The accuracy of the linear interpolation method with the 'no-rotation' discretization approach has already been demonstrated by Cambou *et al*. [4], and the other approaches are also seen to give a good match to the values calculated from the boundary conditions. The non-linear meshfree interpolation over-estimates the lateral displacement gradient values slightly and underestimates the axial displacement gradient values slightly for large strain values.

Three-dimensional case

Both the linear and the non-linear interpolation methods were implemented in three dimensions, and as before the 'no-rotational' and 'rotational' discretizations were considered. A 'servo-controlled' triaxial compression test was used to validate the interpolation approaches. The three-dimensional simulations used a modified version of the three-dimensional DEM code Ellipse3D [12]. The modifications that were made to this code are described in O'Sullivan [22].

The discrete element simulation contained 9000 spherical particles with radii of 0.4, 0.5, and 0.6 cm (ratio of 1:1:1), which were randomly generated in a rectangular box with dimensions 20 cm $\times$ 20 cm $\times$ 40 cm. The particle generation subroutine used is a modified version of the Ellipse 3-D particle generation subroutine. The radii of the spheres were then gradually uniformly expanded to attain a target void ratio of 0.6. A similar approach is used by Itasca [21]. The particles had a scaled density of 2×10^8 kg/m^3. As with the two-dimensional simulation, particle contact was modeled using linear normal and shear springs with a stiffness of 1×10^6 N/m. The interparticle coefficient of friction was 0.3.

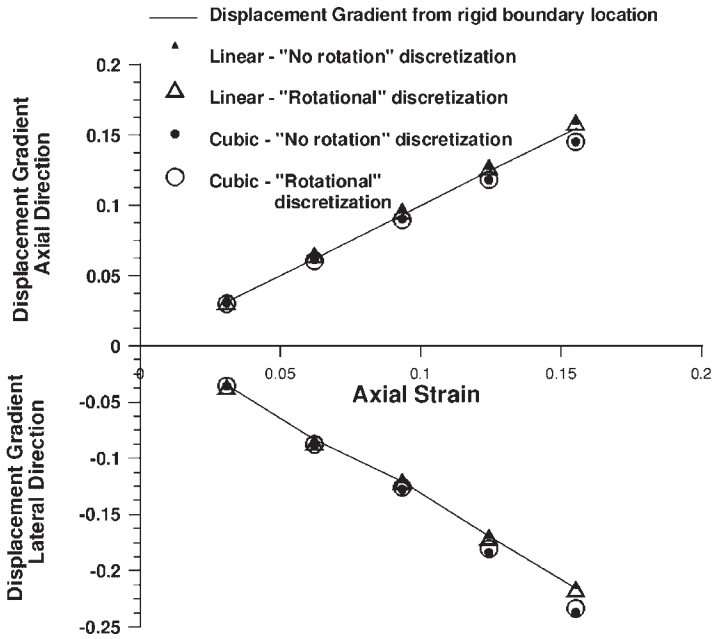

Figure 5. Comparison of golbal and average displacement gradients: Validation of 2-D kinematic averaging approaches.

Once the required void ratio was attained, a measurement sphere, centered at the center of the specimen was created, and the specimen was brought into an isotropic stress state with $\sigma_{xx} = \sigma_{yy} = \sigma_{zz} = 100$ kPa. A 'servo-controlled' system was used to achieve this initial stress state. The void ratio at the start of the triaxial compression test was 0.618. During the simulation the top plate of the box was moved downwards with a constant velocity. The positions of the lateral specimen boundaries were adjusted to maintain constant lateral stresses of $\sigma_{xx} = \sigma_{yy} = 100$ kPa. Figure 6(a) illustrates the initial specimen configuration.

The specimen response is illustrated in Figure 6(b). The stresses were measured using a measurement sphere [1]. The average displacement gradients $\bar{a}_{ii}$ obtained using the linear and non-linear interpolation methods and the 'rotational' discretization are compared with the global displacement gradients, a_{ii}^{global}, (calculated from the boundary conditions) in Figure 7. Overall, a good match is obtained between the a_{ii}^{global} and the $\bar{a}_{ii}$ values for all the homogenization methods examined in this study.

STRAIN LOCALIZATION STUDY

Simulation of dense biaxial compression test

A discrete element simulation of a two-dimensional compression test on a dense specimen of randomly arranged disks was performed to allow evaluation of the ability of the linear and non-linear interpolation approaches to capture the development of a localized shear band. The

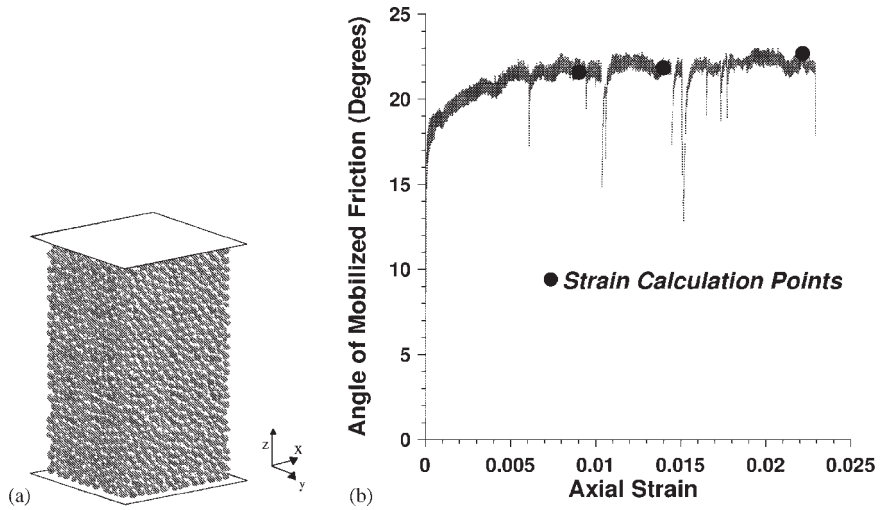

Figure 6. Validation of 3-D kinematic averaging approaches: (a) initial particle configuration and (b) specimen response for 3-D servo controlled triaxial test.

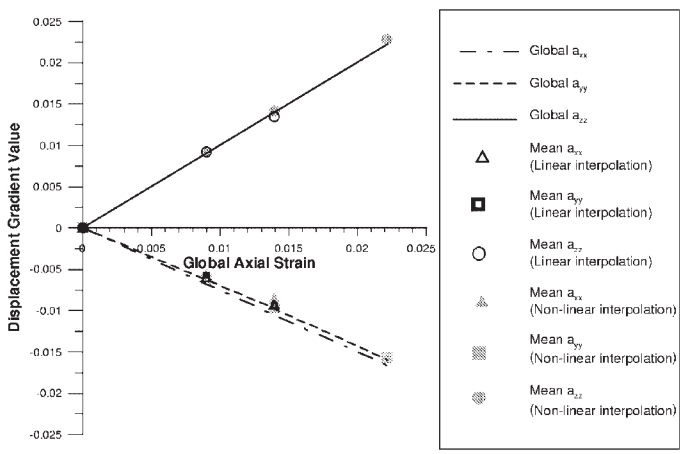

Figure 7. Results of validation of three-dimensional kinematic averaging approaches: Comparison of global displacement gradients and average displacement gradients for linear and non-linear interpolation with 'rotational' discretization.

influence of particle rotation on the calculated shear strain is also investigated for the non-linear meshfree interpolation approach.

The simulation was performed using the two-dimensional DEM code, PFC-2D. The specimen contains 12 512 disks and is illustrated in Figure 8(a). The specimen was created using the specimen generation approaches proposed by Itasca [21]; the particle radii were generated to be uniformly distributed between 0.075 and 0.100 cm and to have an initial porosity of 0.1. The specimen dimensions are 18 cm wide by 36 cm high. The simulation of the biaxial compression

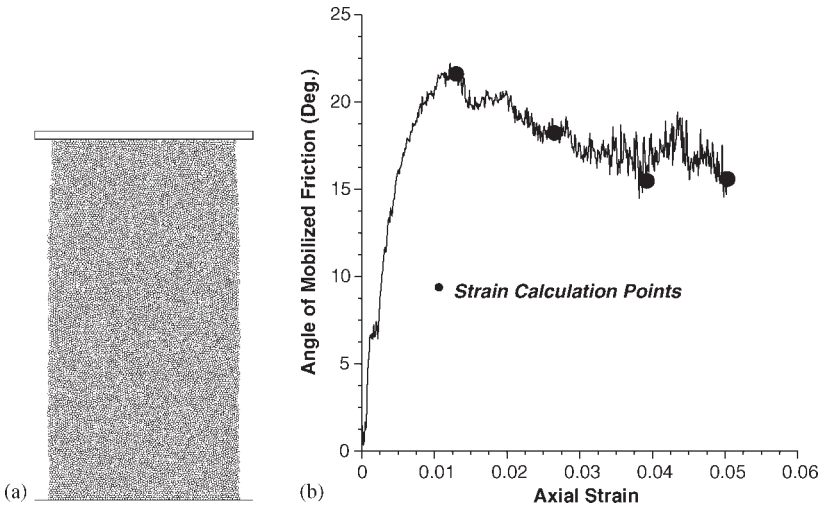

Figure 8. Biaxial test with 12 512 disks: (a) initial disk configuration and (b) specimen response.

test used the 'stress controlled membrane' algorithm proposed by Thomas and Bray [23] and implemented in PFC. The simulation used a scaled particle density of 2×10^9 kg/m^3, linear normal and shear contact springs with a stiffness of 5×10^7 Nm, and an interparticle coefficient of friction of 0.3.

The specimen response plotted as the angle of friction mobilized as a function of axial strain is given in Figure 8(b). The specimen attained a peak angle of mobilized friction of 22.4° at an axial strain of 1.2%. Representative plots of the incremental displacements are given in Figure 9. To aid in the visualization, only the particle displacement vectors whose magnitude exceeds the magnitude of the median particle displacement are shown. At small strain levels, the displacement localizations are not distinguishable; however, with increasing strain, two localization zones can be seen. After the peak stress has been reached, i.e. strains exceeding 1.3%, the localization that dips to the left can be seen more easily.

Considering the particle rotations, at each strain level the mean clockwise particle rotation and the mean counter-clockwise particle rotation were calculated. The rotations that are greater in magnitude than these mean values are then illustrated in Figure 10. The particles whose rotation exceeds the mean counter-clockwise rotation are indicated as solid black circles. The particles whose rotation exceeds the mean clockwise rotation are indicated as hollow circles. In both cases the shear band locations are defined by the locations of the zones of maximum rotation. The trend is for clockwise rotations to dominate in the localizations that dip to the left, while the rotations in the localizations that dip to the right tend to be counter-clockwise. This pattern of rotation direction is similar to the observations of Iwashita and Oda [10]. For circular disks with rotational resistance at the contact points, Iwashita and Oda [10] found that the disks in the shear band dipping to the right experienced clockwise rotation, while the disks in the shear band dipping to the left experienced counter-clockwise rotation. In contrast to the results presented here, Iwashita and Oda [10] found that disks in the specimen with no rotational contact resistance (as is modeled in these simulations) showed no definite tendency to rotate in either direction.

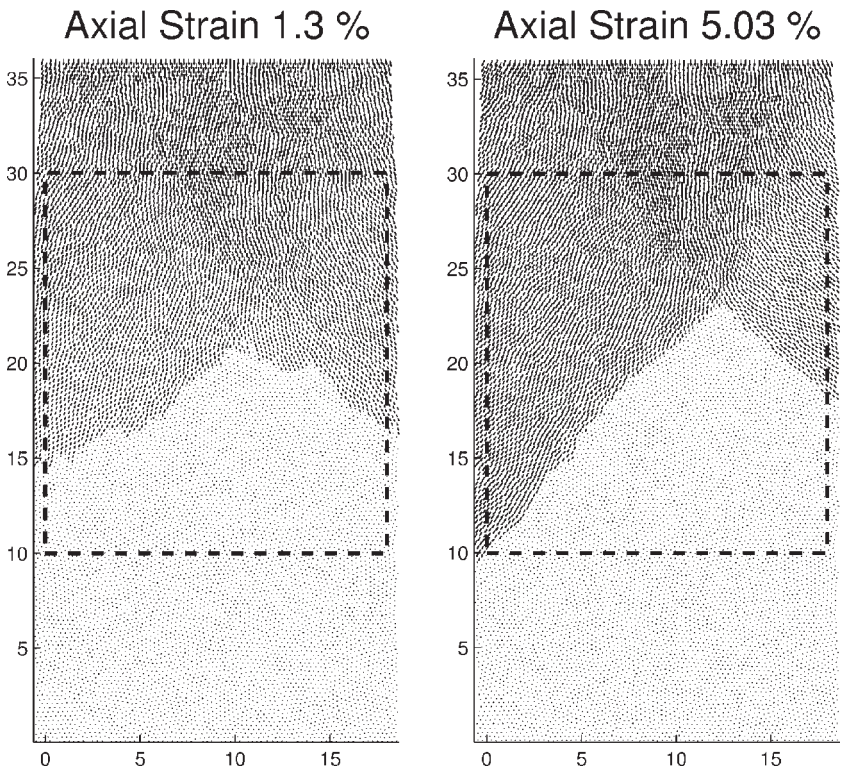

Figure 9. Plot of incremental displacements, for biaxial test with 12 512 disks (Only incremental displacements exceeding the median value are shown). *The rectangular box indicates the area of the specimen for which strain contour plots were developed.*

Evolution of local strain distribution

Three homogenization methods were used to calculate the strain values for this system: linear interpolation with 'no rotation' discretization, non-linear meshfree interpolation with 'no rotation' discretization, and non-linear meshfree interpolation with 'rotational' discretization. For the non-linear meshfree interpolation the window size for the interpolation (w_r) was set to $1 \times r$, where r is the particle radius. For ease of visualization, the strain contours were developed over a portion of the specimen shown in Figure 9 where the shear bands developed. The grid used to calculate the strain values had 100 points in the x-direction and 200 points in the y-direction. For the 'rotational' discretization the measured points were located at 0.9 times the disk radius from the disk centroid.

Contour plots of the calculated shear strains are illustrated in Figure 11 for each of the three cases: (a) linear FEM-type interpolation, (b) non-linear meshfree interpolation with 'no-rotation' discretization and (c) non-linear meshfree interpolation with 'rotational' discretization for the deformed specimen at an axial strain of 2.65%. In these plots, the strain contours are at intervals of 0.25, and the color scale runs from 0 to 4. The linear interpolation approach and the non-linear 'no-rotation' approach yield similar strain contour distributions. However, the

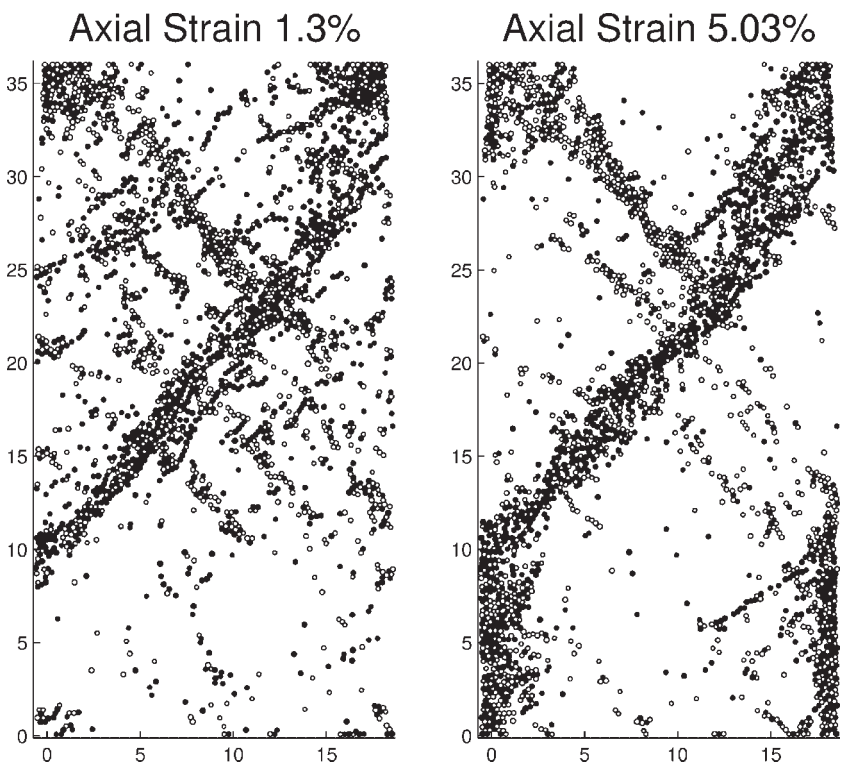

Figure 10. Plot of accumulated rotations, for biaxial test with 12 512 disks. The filled circles indicate clockwise rotation (exceeding the mean clockwise rotation value), while the hollow circles indicate anti-clockwise rotation (exceeding the mean counter-clockwise rotation value).

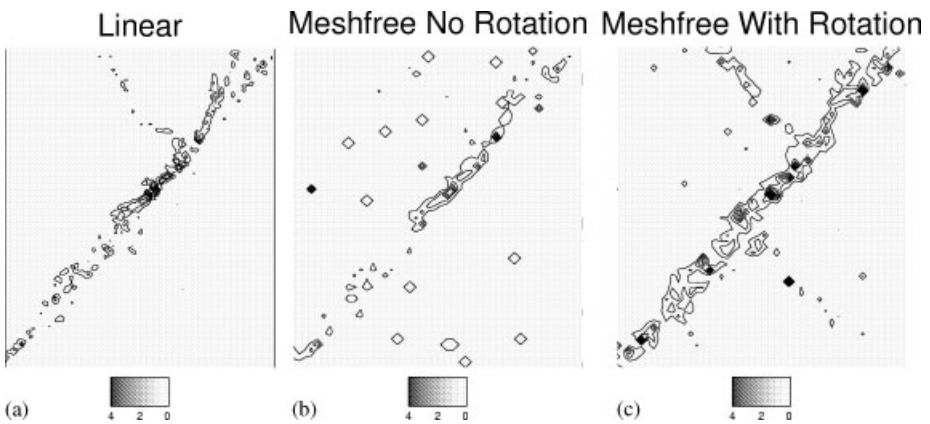

Figure 11. Plot of shear strain contours for biaxial test with 12 512 disks. *The strain values are illustrated by shading*.

non-linear 'rotational' interpolation identifies the secondary regions of localization more effectively than either the linear interpolation approach or the non-linear, 'no-rotation' approach.

The volumetric strain contours are illustrated in Figure 12 for these same three interpolation schemes. There is a significant amount of 'noise' away from the zone of localization. The areas of the specimen that exhibit a contractive response tend to be located away from the localization, while the areas of the specimen that exhibit a more dilative response are located closer to the localization. The shape of the localization is similar for all three schemes. However, the non-linear interpolation with the 'rotational' discretization produces a localization that is longer in extent at an axial strain of 2.65% in comparison to the other two cases.

Considering the strain contour plots shown in Figures 11 and 12, it is important to realize that for the non-linear meshfree interpolation approach the results are somewhat sensitive to the size of the widow used in the interpolation function. The strain calculations were repeated using a window size of $w = 2 \times r$, where r is the particle radius. The maximum strain values obtained

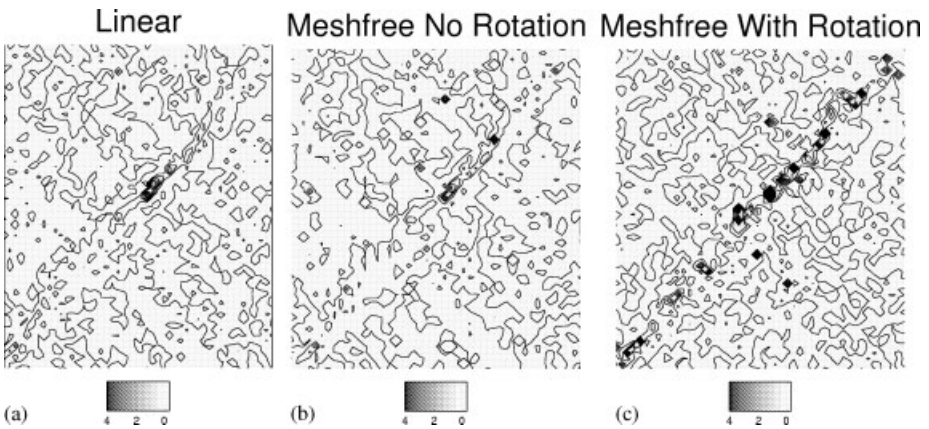

Figure 12. Plot of volumetric strain contours for biaxial test with 12 512 disks. *The strain values are illustrated by shading.*

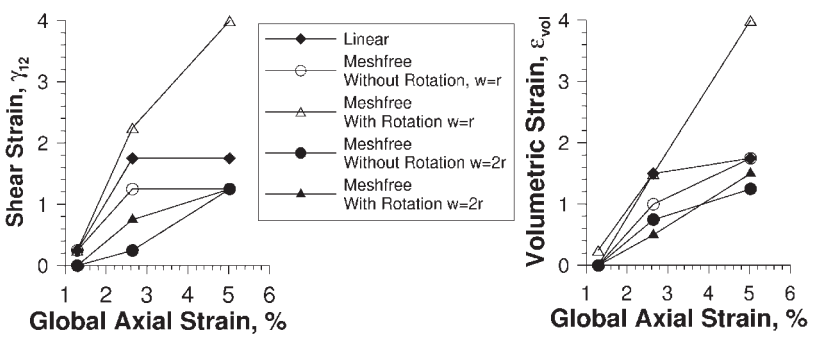

Figure 13. Comparison of maximum strain values for window sizes $w = 1 \times r$ and $w = 2 \times r$, for biaxial test with 12 512 disks.

with each approach are provided in Figure 13. The maximum strain values calculated with the larger window size are significantly smaller than those calculated with the smaller window size, and these values are now less distinguishable from those calculated using the other interpolation schemes. The strain contour distributions were also affected by the window size. In comparison to the results obtained using a window size of $1 \times r$, the effects of particle rotation on the calculated shear values are no longer apparent for larger window size. The narrow width of the shear band for this particular problem requires a restricted window size to capture the localization and to examine the effects of particle rotations on the strain values.

CONCLUSIONS

New approaches to kinematic homogenization for interpreting the results of discrete element simulations have been presented. This work was motivated by the inability of the currently available methods of kinematic homogenization to capture effectively particle rotations. In addition, all of these pre-existing strain calculation methods used some type of local, linear interpolation. Moreover, the effectiveness of these methods to capture the development of localizations in granular materials has not been examined widely. Lastly, while the existing methods of strain calculation were known to be theoretically applicable in three dimensions, the three-dimensional formulations had not been implemented.

In this paper, a simple approach for discretization of the granular material, which can capture particle rotations, has been proposed, and details for both the two-dimensional and three-dimensional implementations of this approach were presented. Using the meshfree interpolants, a non-linear interpolation approach has also been developed and implemented in two and three dimensions. In addition, the linear (FEM-type) interpolation method (currently the most popular interpolation approach in two dimensions) was extended to three dimensions. Simulations were then carried out in both two and three dimensions to validate the proposed kinematic homogenization methods.

A simulation of a biaxial compression test on a dense specimen of circular disks was carried out to compare the strain values calculated using the proposed methods. Several distinct localizations developed in this specimen after the peak strength was mobilized. Considering the larger-scale simulations with irregular packing, the linear interpolation approach gave results that were similar to the non-linear interpolation approach when the 'no-rotation' discretization was employed in both cases. However, the effects of particle rotation on the calculated strain values were found to be important. Strain localizations could be more easily visualized when the non-linear meshfree interpolation approach with 'rotational' discretization was adopted. In addition, the amount of dilation within the localization zone, as well as the shear strain in the localization zone, increased when the particle rotation effects were taken into account. However, the results of the meshfree interpolation are sensitive to the size of the compact support of the window function. As the support size increases, the calculated maximum strain values decrease and the localization becomes less well defined. The sensitivity to the support of the window function size appears to decrease as the extent of the localization (relative to the particle radius) increases. Other researchers who have developed techniques to examine the evolution of local variables in granular materials have observed similar sensitivities to the size of the control volume used to monitor the variable in question.

These approaches also have applicability beyond interpreting the results of discrete element simulations. A number of researchers (e.g. References [9,24]) are using image analysis techniques to study the development of localizations in soil. Because three-dimensional image analysis of granular materials is difficult, researchers have found it is more tractable to consider two-dimensional projections of the three-dimensional particles. The kinematic homogenization methods proposed here could be used in conjunction with such image analysis studies to explore the development of localizations in granular materials in experimental studies.

ACKNOWLEDGEMENTS

Funding for this work has been provided by The O'Reilly Foundation and The David and Lucile Packard Foundation. Prof. Ng of the University of New Mexico provided the source code for the program Ellipse3D.

REFERENCES

1. Bardet, J-P. Introduction to computational granular mechanics. In *Behaviour of granular materials*, Cambou B. (ed.), No. 385 in CISM Courses and Lectures. Springer: Wien, New York, 1998; 99–170.
2. Bagi K, Bojtar I. Different microstructural strain tensors for granular materials. In *Proceedings of the Fourth International Conference on Analysis of Discontinuous Deformation*, Bicanic N (ed.). University of Glasgow: UK, 2001; 261–271.
3. Dedecker F, Chaze M, Dubujet P, Cambou B. Specific features of strain in granular materials. *Mechanics of Cohesive-Frictional Materials* 2000; **5**:173–193.
4. Cambou B, Chaze M, Dedecker F. Change of scale in granular materials. *European Journal of Mechanics. Vol. A* (*Solids*) 2000; **19**:999–1014.
5. Zienkiewicz O, Taylor R. *The Finite Element Method, Volume 2: Solid Mechanics* (5th edn). Butterworth Heinemann: Oxford, 2000.
6. Thomas PA. Discontinuous deformation analysis of particulate media. *Ph.D. Thesis*, Department of Civil Engineering, University of California: Berkeley, 1997.
7. Calvetti F, Combe G, Lanier J. Experimental micromechanical analysis of a 2D granular material: relation between structure evolution and loading path. *Mechanics of Cohesive–Frictional Materials* 1997; **2**:121–163.
8. Liao C, Chang T, Young D, Chang C. Stress-strain relationships for granular materials based on the hypothesis of best fit. *International Journal of Solids and Structures* 1997; **34**:4087–4100.
9. Oda M, Kazama H. Microstructure of shear bands and its relation to the mechanisms of dilatancy and failure of dense granular soils. *Geotechnique* 1998; **48**(4):465–481.
10. Iwashita K, Oda M. Micro-deformation mechanism of shear banding process based on modified distinct element method. *Powder Technology* 2000; **109**:192–205.
11. Masson S, Martinez J. Micromechanical analysis of the shear behavior of a granular material. *ASCE Journal of Engineering Mechanics* 2001; **127**(10):1007–1016.
12. Lin X, Ng T.-T. A three-dimensional discrete element model using arrays of ellipsoids. *Geotechnique* 1997; **47** (2):319–329.
13. Zienkiewicz O, Taylor R. *The Finite Element Method, Volume 1: The Basis* (5th edn). Butterworth Heinemann: Oxford, 2000.
14. Belytschko T, Krongauz Y, Flemind D, Krysl P. Meshless methods: An overview and recent developments. *Computer Methods in Applied Mechanics and Engineering* 1996; **139**(2–4):3–47.
15. Li S, Liu WK. Meshfree particle methods and their applications. *Applied Mechanics Review* 2002; **54**:1–34.
16. Li S, Liu WK. Numerical simulations of strain localization in inelastic solids using meshfree methods. *International Journal for Numerical Methods in Engineering* 2000; **48**:1285–1309.
17. Murakami A, Kawabata H, Aoyama S. EFGM analysis for saturated soil. In *Computer Methods and Advances in Geomechanics*, Desai *et al*. (eds). Balkema: Rotterdam, 2001; 153–156.
18. Horner DA. Application of DEM to micro-mechanical theory for large deformations of granular media. *Ph.D. Thesis*, University of Michigan, 1997.
19. Liu WK, Jun S, Zhang YF. Reproducing kernel particle methods. *International Journal of Numerical Methods in Fluids* 1995; **20**:1081–1106.
20. Liu WK, Li S, Belytschko T. Moving least square kernel method. 1: Methodology and convergence. *Computer Methods in Applied Mechanics and Engineering* 1997; **143**:113–154.

21. Itasca Consulting Group. *PFC2D 2.00 Particle Flow Code in Two Dimensions*. Itasca Consulting Group, Inc.: Minneapolis, Minnesota, 1998.
22. O'Sullivan, C. The application of discrete element modeling to finite deformation problems in geomechanics. *Ph.D. Thesis*, Department of Civil Engineering, University of California: Berkeley, 2002.
23. Thomas PA, Bray JD. Capturing the Nonspherical Shape of Granular Media with Disk Clusters. *ASCE*, *Journal of Geotechnical and Geoenvironmental Engineering* 1999; **125**(3):169–178.
24. Frost JD, Jang DJ. Evolution of Sand Microstructure During Shear. *ASCE*, *Journal of Geotechnical and Geoenvironmental Engineering* 2000; **126**(2):116–130.

